CrossMark

J. Fluid Mech. (2016), *vol.* 808, R2, doi:10.1017/jfm.2016.660

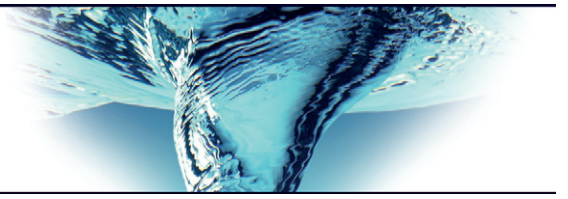

The rapid-rotation limit of the neutral curve for Taylor–Couette flow

Kengo Deguchi†

School of Mathematical Sciences, Monash University, VIC 3800, Australia

(Received 11 August 2016; revised 7 October 2016; accepted 10 October 2016;
first published online 27 October 2016)

An asymptotic theory is developed for the linear stability curve of rapidly rotating Taylor–Couette flow. The analytic curve obtained by the theory excellently explains the limiting Navier–Stokes stability result for general disturbances. When the cylinders are corotating, the asymptotic theory describes the gap between the neutral curve and the Rayleigh stability criterion. For the case when the cylinders are counter-rotating, it is found that, along the stability boundary, the Reynolds number based on the inner cylinder speed is proportional to that based on the outer cylinder speed to the power of 3/5.

Key words: high-speed flow, Taylor–Couette flow

1. Introduction

Taylor–Couette flow has long served as a theoretical testing ground for the stability theory of rotating fluid flows. Linear stability theory is probably one of the greatest theoretical achievements developed using the apparatus; the theory has been treated by a number of authors since Taylor (1923) established the excellent agreement of the stability analysis based on the Navier–Stokes equations with the experimental results of fluid flows between independently rotating concentric cylinders. The neutral curve derived from the linear stability analysis significantly improved the accuracy of the stability boundary of the basic flow from the previously established Rayleigh stability criterion derived assuming inviscid and axisymmetric properties of the disturbances (Rayleigh 1917).

The stability diagram of Taylor–Couette flow for the radius ratio $\eta = 5/7$ (used in recent experiments/simulations, for example, Ostilla *et al.* 2013) is shown in figure 1. The stability of the flow is computed over a range of inner and outer Reynolds numbers, R_i and R_o, respectively. The grey region is the area called the Rayleigh stable region, where the quantity called the Rayleigh discriminant becomes negative for all radial positions. The neutral curve sits inside the Rayleigh unstable region as

† Email address for correspondence: Kengo.Deguchi@monash.edu

© Cambridge University Press 2016

https://doi.org/10.1017/jfm.2016.660 Published online by Cambridge University Press

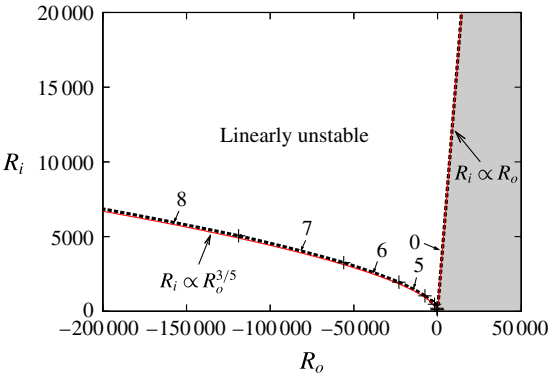

FIGURE 1. The stability of Taylor–Couette flow for $\eta = 5/7$. The thick dashed curve is the neutral curve obtained from the linear stability analysis of the Navier–Stokes equations. The axial and azimuthal wavenumbers are optimised to give the most unstable result. The crosses on the neutral curve are the bicritical points, where the value of the optimised azimuthal wavenumber indicated by the arrows changes. The red solid curves are the asymptotic result. Corotation case ($R_iR_o > 0$): Rayleigh line $R_i = \eta^{-1}R_o$. Counter-rotation case ($R_iR_o < 0$): $R_i = C_2|R_o|^{3/5}$ with $C_2(\eta)$ shown in figure 6(*b*). The grey region is Rayleigh stable. The boundary of the Rayleigh stable region is defined by the Rayleigh line $R_i = \eta^{-1}R_o$ and $R_i = 0$.

shown by the dashed curve, and the gap between the linear and Rayleigh stability boundaries is called the viscous correction. When the basic flow is linearly unstable, cellular fluid motions develop due to the centrifugal instability. In the R_i–R_o plane, various cellular patterns have been observed, as shown in the seminal experimental work of Andereck, Liu & Swinney (1986). More recently, the parameter dependence of the Taylor–Couette flow for higher Reynolds numbers has been of great concern, as summarised in the review paper by Grossmann, Lohse & Sun (2016). The linear stability boundary accurately describes the onset of these nonlinear patterns as long as the disturbances are so small that the possibility of subcritical instability (see Deguchi, Meseguer & Mellibovsky (2014), for example) is excluded.

The aim of this short paper is to produce a rational analytic expression for the limiting neutral curve for rapidly rotating Taylor–Couette flow. Previously, the derivation of such analytic approximations has been attempted by Esser & Grossmann (1996) and Dutcher & Mullar (2007). However, despite the nice physical insights introduced, the results in those papers are entirely based on *ad hoc* assumptions and thus are not compatible with the high-Reynolds-number approximation to the Navier–Stokes equations. So far, rational asymptotic theory of the neutral curve is limited for the case of a stationary outer cylinder (Hall 1982). Although it is well known that when the cylinders are rotating in the same direction (the corotating case) the most unstable disturbance is axisymmetric and the neutral curve is asymptotic to the Rayleigh line, the analysis of the viscous correction by a self-consistent high-Reynolds-number asymptotic analysis has not been performed. When the cylinders are rotating in opposite directions (the counter-rotating case), the limiting behaviour is less clear since the most unstable disturbance has a non-zero azimuthal wavenumber (see Langford *et al.* 1988) and thus does not satisfy the assumptions made in Rayleigh's stability analysis.

In the next section we start our analysis for a simplified problem valid for axisymmetric disturbances at the narrow-gap limit ($\eta \to 1$). Section 3 generalises

https://doi.org/10.1017/jfm.2016.660 Published online by Cambridge University Press

the asymptotic theory derived in § 2. Lastly, in § 4, we draw some conclusions and discuss the implications of the asymptotic analysis.

2. Axisymmetric vortices in narrow-gap cylinders

Consider a Taylor–Couette flow governed by the incompressible Navier–Stokes equations in infinitely long rotating concentric cylinders with radius ratio $\eta < 1$. Following convention, the gap and fluid density are scaled to be unity. The viscous velocity scale is chosen for the velocity components, and thus the Reynolds numbers appear in the boundary conditions rather than in the governing equations. Hence, in cylindrical coordinates (r, θ, z), the normalised azimuthal velocity V must satisfy the no-slip conditions on the cylinder walls:

$$V = R_i \quad \text{at } r_i \equiv \eta/(1-\eta), \tag{2.1a}$$

$$V = R_o \quad \text{at } r_o \equiv 1/(1-\eta), \tag{2.1b}$$

where R_i and R_o are the cylinder speeds non-dimensionalised by the kinematic viscosity of the fluid and the gap.

In this section we assume that the disturbance is axisymmetric. Defining the streamfunction φ, where the radial and axial velocity components U and W are written as $-\varphi_z$ and $r^{-1}(r\varphi)_r$, respectively, the Navier–Stokes equations become

$$V_t + r^{-2}\{(r\varphi)_r(rV)_z - (r\varphi)_z(rV)_r\} = \Delta V, \tag{2.2a}$$

$$\Delta\varphi_t + (r\varphi)_r\left(\frac{\Delta\varphi}{r}\right)_z - (r\varphi)_z\left(\frac{\Delta\varphi}{r}\right)_r = \Delta^2\varphi - \frac{2VV_z}{r}. \tag{2.2b}$$

Here note that $-\Delta\varphi = -(\varphi_{rr} + r^{-1}\varphi_r - r^{-2}\varphi + \varphi_{zz})$ describes the streamwise vorticity. In order to perform the stability analysis, we linearise the governing equations around the basic flow $V = V_b(r)$,

$$V_b(r) = Ar + Br^{-1}, \quad A \equiv \frac{R_o - \eta R_i}{1+\eta}, \quad B \equiv \frac{\eta^{-1}R_i - R_o}{1+\eta}r_i^2. \tag{2.3a–c}$$

We further simplify the equations by taking the narrow-gap limit $\eta \to 1$. Since we have fixed the gap to be unity, the limit corresponds to $r_i, r_o \sim (1-\eta)^{-1} \to \infty$. Thus we define an $O((1-\eta)^0)$ gap variable $y = r - \bar{r}$ with some representative radius $\bar{r} \in [r_i, r_o]$, which is of course $O((1-\eta)^{-1})$. In order to take the limit, it is convenient to write $V = V_b + 2Av$ in (2.2) with the scaled velocity v, to get

$$v_t + r^{-2}\{(r\varphi)_r(rv)_z - (r\varphi)_z(rv)_r\} = \Delta v + \varphi_z, \tag{2.4a}$$

$$\Delta\varphi_t + (r\varphi)_r\left(\frac{\Delta\varphi}{r}\right)_z - (r\varphi)_z\left(\frac{\Delta\varphi}{r}\right)_r = \Delta^2\varphi - \frac{8A^2 v v_z}{r} + \Xi v_z, \tag{2.4b}$$

where $\Xi(r) \equiv -4AV_b/r$ is called the Rayleigh discriminant. In order to keep the terms on the right-hand side of (2.4*a*), we see that $\partial_z \sim O(\bar{r}^0)$, and that v and φ are comparable in size. Then, when $\bar{r} \gg y$, the Rayleigh discriminant on the right-hand side of (2.4*b*) expands to

$$\Xi = -\frac{4A\overline{V}_b}{\bar{r}}\left(1 - 2\frac{y}{\bar{r}}\right) - 8A^2\left(\frac{y}{\bar{r}}\right) + O(\bar{r}^{-2}), \tag{2.5}$$

where $\overline{V}_b \equiv V_b(\bar{r}) = \gamma R_o + (1-\gamma)R_i$ and $\gamma \equiv \bar{r} - r_i$. Here γ is chosen to be $1/2$ for later convenience. If we assume $T \equiv -4A\overline{V}_b/\bar{r}$ and $G \equiv 8A^2/\bar{r}$ are $O(\bar{r}^0)$, then $\Xi \to [T - Gy] \sim O(\bar{r}^0)$ as $\eta \to 1$. Therefore, assuming an infinitesimally small disturbance

https://doi.org/10.1017/jfm.2016.660 Published online by Cambridge University Press

of normal mode form $(v, \varphi) = (\widetilde{v}, \widetilde{\varphi}) \exp[\sigma t + \mathrm{i}kz]$ with $\widetilde{v} = \widetilde{\varphi} = \partial_y \widetilde{\varphi} = 0$ on the cylinder walls, we have the eigenvalue problem for a complex growth rate σ:

$$0 = \{(\partial_y^2 - k^2) - \sigma\}\widetilde{v} + \mathrm{i}k\widetilde{\varphi}, \tag{2.6a}$$

$$0 = \{(\partial_y^2 - k^2) - \sigma\}(\partial_y^2 - k^2)\widetilde{\varphi} + \mathrm{i}k[T - Gy]\widetilde{v}. \tag{2.6b}$$

This problem can be solved numerically by the Chebyshev collocation method to obtain the stability curve in terms of (T, G). In order to compare the stability to that for the wide-gap cases, it is convenient to rescale R_i and R_o as

$$R_i^+ \equiv R_i\sqrt{1-\eta} = (2G)^{-1/2}\Xi|_{r=r_i} = (2G)^{-1/2}(T + G/2), \tag{2.7a}$$

$$R_o^+ \equiv R_o\sqrt{1-\eta} = (2G)^{-1/2}\Xi|_{r=r_o} = (2G)^{-1/2}(T - G/2). \tag{2.7b}$$

These scaled Reynolds numbers are $O(\bar{r}^0)$ if $T, G \sim O(\bar{r}^0)$ and therefore, as shown in figure 2, in the R_i^+–R_o^+ plane the neutral curve for the wide-gap case converges to the narrow-gap result as $\eta \to 1$.

Now, let us perform a rapid-rotation asymptotic analysis of (2.6). First we focus on the corotating case. For this case, we may assume that $|B|$ is large but $|A|$ is small, since we already know that the neutral curve is close to the Rayleigh line where $A = 0$. In the context of the narrow-gap limit, this means that we are concerned with the limit of small G/T. This special case corresponds to the rotating plane Couette flow (RPCF) investigated, for example, by Nagata (1986). For the RPCF, $\bar{r}$ is taken at the midgap, and thus we have chosen γ to be $1/2$. It is noteworthy that, as is well known, streamwise independent RPCF has an exact analogy to Rayleigh–Bénard convection, and the Rayleigh discriminant, which now becomes a constant called the Taylor number T, plays the role of the Rayleigh number (Veronis 1970). In this analogy, a positive/negative Rayleigh discriminant corresponds to an unstable/stable stratification. In figure 2, the results for RPCF are plotted as the blue solid curve using the well-known critical value of the Taylor number $T = 1707.8 = R_i^{+2} - R_o^{+2}$. Near the Rayleigh line $R_i^+ \approx R_o^+$, and the asymptotic stability curve is written as

$$R_i^+ = R_o^+ + \frac{T}{2R_o^+} + \cdots. \tag{2.8}$$

It is now clear that the Taylor number describes the leading-order effect of the viscous correction.

On the other hand, the neutral curve for the counter-rotating case corresponds to the limit of large G/T; also recall that it appears near the other boundary of the Rayleigh stable region, $R_i = 0$. The normalised Rayleigh discriminant at sufficiently large G along the neutral curve of (2.6) is shown in figure 3. This time, the discriminant is not uniform, but a monotonically decreasing function in r with the positive part concentrated near the inner cylinder. As expected from the analogy to the convection problem, we see that it is this positive part that drives the near-wall instability shown by the streamfunction. This observation motivates the asymptotic analysis of the limiting neutral curve for the case of counter-rotation. Assuming that G is asymptotically large and all the disturbances are concentrated near the inner cylinder, we analyse the stability in the near-wall layer where the stretching variable $Y = \delta^{-1}(y + 1/2)$ is $O(1)$. The thickness of the boundary layer $\delta \ll 1$ is to be fixed in terms of G. If we assume that the positive part of $\Xi = G[(T/G + 1/2) - \delta Y]$ is concentrated in the wall layer, the small positive constant part and the term

https://doi.org/10.1017/jfm.2016.660 Published online by Cambridge University Press

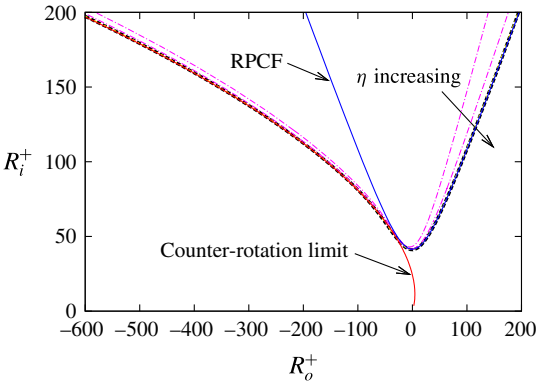

FIGURE 2. The stability of Taylor–Couette flow under axisymmetric disturbances. The value of the axial wavenumber is optimised. The rescaled parameters R_i^+ and R_o^+ are defined in (2.7). The magenta dot-dashed curve represents the results for $\eta = 5/7, 0.9, 0.99$. The result for $\eta = 0.99$ is almost indistinguishable from the narrow-gap results indicated by the black thick dashed curve. The red and blue solid curves are asymptotic results for the narrow-gap limit.

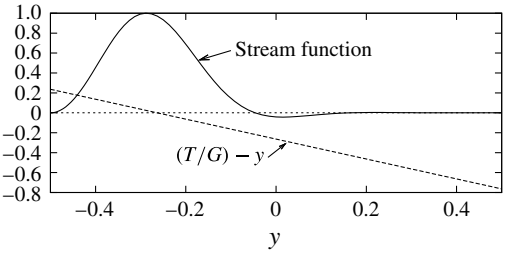

FIGURE 3. The solid curve is the neutral disturbance of the narrow-gap limit equations (2.6) at $(G, T, k) = (1.6 \times 10^6, -1.22 \times 10^6, 8.6)$. The dashed line is the corresponding normalised Rayleigh discriminant $\Xi/G = T/G - y$.

proportional to Y must be comparable in size. Thus we define an $O(1)$ quantity $Q_0 = \delta^{-1}(T/G + 1/2)$ to write $\Xi = \delta G[Q_0 - Y]$. We further define the scaled wavenumber $k_0 = \delta k$ to balance the wall-normal and spanwise diffusion. From the scaling, k is asymptotically large, and this is indeed the case in view of the computational result. Likewise, we write the scaled growth rate as $\sigma_0 = \delta^2\sigma$. Substituting the scaled variables and the expansions $\widetilde{\varphi} = \delta^{-1}\widetilde{\varphi}_0 + \cdots$, $\widetilde{v} = \widetilde{v}_0 + \cdots$ into (2.6), we get the leading-order problem

$$0 = \{(\partial_Y^2 - k_0^2) - \sigma_0\}\widetilde{v}_0 + \mathrm{i}k_0\widetilde{\varphi}_0, \tag{2.9a}$$

$$0 = \{(\partial_Y^2 - k_0^2) - \sigma_0\}(\partial_Y^2 - k_0^2)\widetilde{\varphi}_0 + \mathrm{i}k_0(\delta^5 G)[Q_0 - Y]\widetilde{v}_0, \tag{2.9b}$$

$$\widetilde{\varphi}_0 = \widetilde{\varphi}_{0Y} = \widetilde{v}_0 = 0, \quad \text{at } Y = 0, \infty. \tag{2.9c}$$

The balance in the second equation gives the layer thickness $\delta = G^{-1/5}$. The problem (2.9) can be solved by a standard linear eigenvalue solver to seek the neutral point where the real part of σ_0 vanishes. Here the equations are discretised by

https://doi.org/10.1017/jfm.2016.660 Published online by Cambridge University Press

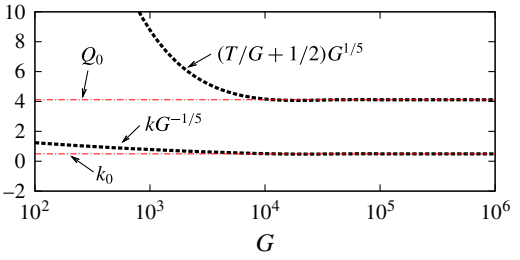

FIGURE 4. The thick dashed curves are the neutral curve of the narrow-gap problem (2.6) and the optimised value of k. These results are rescaled by the near-wall-layer thickness $G^{-1/5}$. The dot-dashed lines are the large-G asymptotic results $Q_0 = 4.11$ and $k_0 = 0.494$ computed using (2.9).

the Chebyshev collocation method in Y, mapping $[0, \infty]$ to $[-1, 1]$; see Boyd (2001), for example. The accuracy of the computation has been checked by changing the number of collocation points, typically taking more than 200. Along the computed neutral curve $Q_0(k_0)$, we minimise the value of Q_0 to yield the critical point $(Q_0, k_0) = (4.11, 0.494)$. As shown in figure 4, the scaled Navier–Stokes result computed by (2.2) quickly converges to the asymptotic result when increasing the value of G. The asymptotic result can also be confirmed in figure 2, where the result is presented in terms of R_i^+ and R_o^+ based on the critical value transformed using the definition of Q_0 and (2.7). We can see that the asymptotic result shown by the red solid curve excellently approximates the counter-rotating limit of the Navier–Stokes result.

3. General case

On the basis of the basic physics of the instability given in the previous section, we now generalise the theory to a wide gap and arbitrary linear disturbances. In order to generalise the asymptotic results we introduce the toroidal–poloidal potential decomposition

$$\begin{aligned}(U, V, W) &= V_b \boldsymbol{e}_\theta + \boldsymbol{\nabla} \times \boldsymbol{\nabla} \times (\phi \boldsymbol{e}_r) + \boldsymbol{\nabla} \times (\psi \boldsymbol{e}_r) \\ &= (-\Delta_2 \phi,\, V_b + \partial_{r\theta} r^{-1} \phi + \partial_z \psi,\, r^{-1} \partial_{rz} r \phi - \partial_\theta r^{-1} \psi),\end{aligned} \tag{3.1}$$

where $\Delta_2 \equiv r^{-2}\partial_\theta^2 + \partial_z^2$ is the two-dimensional Laplace operator. The linearised Navier–Stokes equations can then be written in the form (see Deguchi & Nagata 2011, for example)

$$\begin{aligned}0 &= -r(\partial_t - \Delta_{3'})\Delta_2 \frac{\psi}{r} + \frac{2}{r^2}\partial_r \frac{\psi_{\theta\theta}}{r} + \frac{2}{r}(\partial_t - 2\Delta_3)\frac{\phi_{\theta z}}{r} \\ &\quad + (rV_b)'\partial_z \Delta_2 \frac{\phi}{r} + \frac{V_b}{r}\partial_\theta \left(\frac{2}{r^2}\phi_{\theta z} - \Delta_2 \psi\right),\end{aligned} \tag{3.2a}$$

$$\begin{aligned}0 &= r(\partial_t - \Delta_{3'})\left(\Delta_{3'}\Delta_2 \frac{\phi}{r} + \frac{2}{r^3}\partial_r \frac{\phi_{\theta\theta}}{r}\right) - \frac{2}{r^2}\left(\partial_r \Delta_3 \frac{\phi_{\theta\theta}}{r} - \frac{2}{r^2}\phi_{\theta\theta zz}\right) + \frac{2}{r}(\partial_t - 2\Delta_3)\frac{\psi_{\theta z}}{r} \\ &\quad + \frac{V_b}{r}\partial_\theta \left(r\Delta_2\Delta_3 \frac{\phi}{r} + 2\partial_r \frac{\phi_{zz}}{r} + \frac{2}{r^2}\psi_{\theta z}\right) + \left(\frac{V_b'}{r} - V_b''\right)\partial_\theta \Delta_2 \frac{\phi}{r} \\ &\quad - \frac{2}{r^2}V_b' \Delta_2 \phi_\theta - \frac{3}{r^3}V_b \phi_{\theta zz} + \frac{1}{r^5}V_b \phi_{\theta\theta\theta} + \frac{2}{r}V_b \Delta_2 \psi_z,\end{aligned} \tag{3.2b}$$

https://doi.org/10.1017/jfm.2016.660 Published online by Cambridge University Press

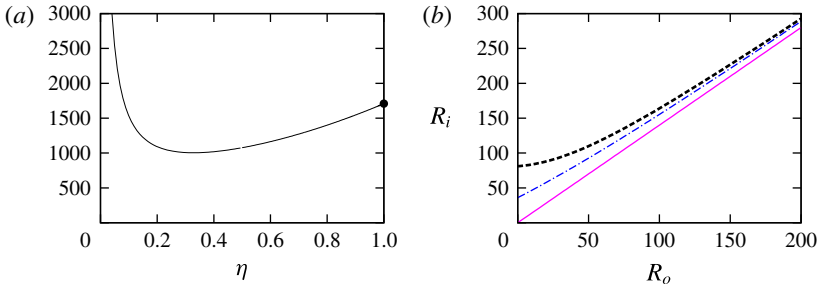

FIGURE 5. The asymptotic results for the corotating case. (*a*) The coefficient C_1 in (3.3). The filled circle is the narrow-gap result $C_1 = 1707.8$. (*b*) Comparison of the neutral curve for $\eta = 5/7$ (black dashed curve) and the asymptotic prediction (3.4) truncated at the second term (blue dot-dashed curve). The magenta solid line is the Rayleigh line $R_i = \eta^{-1} R_o$.

where

$$\Delta_3 \equiv \partial_r^2 + \frac{1}{r}\partial_r + \Delta_2, \quad \Delta_{3'} \equiv \partial_r^2 + \frac{3}{r}\partial_r + \Delta_2. \tag{3.2c,d}$$

If the flow is axisymmetric, i.e. $\partial_\theta = 0$, we recover (2.2) with the replacement of (φ, V) by $(\phi_z, V_b + \psi_z)$.

It is known that the most unstable mode for the corotating case is axisymmetric and the neutral curve approaches the Rayleigh line, where the value of $|A|$ is small and that of $|B|$ is large. It is reasonable to assume the size of A is $O(B^{-1})$, because by substituting the Rayleigh discriminant and the basic flow (2.3), we see that the right-hand side of (2.4) depends on A^2 and (AB). Then we can numerically seek the critical value of (AB), neglecting the terms proportional to A^2. Assuming φ and v are $O(1)$, no other term drops from (2.4) at the asymptotic limit. Thus the vortices are fully viscous, in the sense that the leading-order perturbation at the limit can be determined only by the viscous problem. Using the critical value we can calculate the coefficient

$$C_1(\eta) \equiv -\frac{AB(1+\eta)^2\eta}{r_i^2} = (\eta R_i - R_o)(R_i - \eta R_o). \tag{3.3}$$

As shown in figure 5(*a*), reducing η from the narrow-gap value 1, the value of C_1 decreases from 1707.8 (shown by the filled circle, the same value as the critical Taylor number at the RPCF limit) and then reaches a minimum at $\eta \approx 0.33$. Upon further decreasing η, the curve shown in the figure tends to infinity as $\eta \to 0$. The value of C_1 gives the asymptotic prediction

$$R_i = \frac{R_o}{\eta} + \frac{C_1}{1-\eta^2} R_o^{-1} + \cdots \tag{3.4}$$

in R_i–R_o parameter space; this is a generalisation of (2.8). In figure 5(*b*), the Navier–Stokes result and the asymptotic prediction are compared for $\eta = 5/7$. As in the last section, the asymptotic result describes the gap between the neutral curve and the Rayleigh line.

Next we shall analyse the counter-rotating case, writing the potentials in their normal mode form $(\phi, \psi) = (\widetilde{\phi}, \widetilde{\psi}) \exp[\sigma t + \mathrm{i}m\theta + \mathrm{i}kz]$. As in the previous section,

https://doi.org/10.1017/jfm.2016.660 Published online by Cambridge University Press

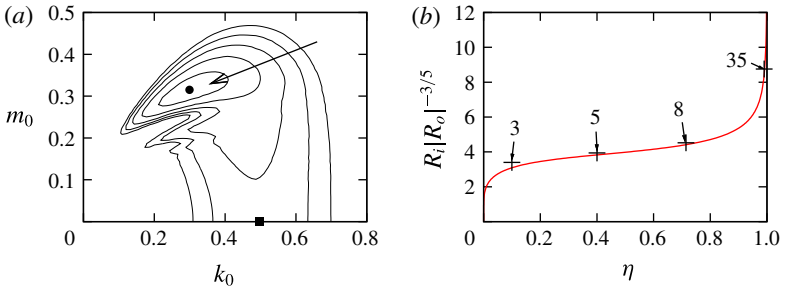

FIGURE 6. The asymptotic results for the counter-rotating case. (*a*) The neutral solution of the asymptotic problem (3.7). The contours indicate $Q_0 = 4.3$, 4.2, 4.1, 4.0 and 3.9. The value of Q_0 decreases in the direction of the arrow and takes the minimum value $Q_0 = 3.85$ at $(k_0, m_0) = (0.300, 0.315)$ as indicated by the circle. The square corresponds to the minimum of Q_0 for the axisymmetric case. (*b*) The comparison of the asymptotic and full Navier–Stokes stability. The solid curve is the asymptotic result C_2 given in (3.8). The crosses are the neutral point at $R_o = -2 \times 10^5$ based on the Navier–Stokes computations. The arrows indicate the values of the optimum azimuthal wavenumber m used in the computation.

we may seek an asymptotic problem near the inner cylinder with asymptotically large axial wavenumber k. From numerical observations, the azimuthal wavenumber m also increases asymptotically (see figure 1) but at a smaller rate than k. Thus we assume $\delta^{-1} \sim k \gg m \gg 1$ in (3.2) and neglect small terms, to get

$$0 = \{(\delta^{-2}\partial_Y^2 - k^2) - \sigma - \mathrm{i}mr^{-1}V_b\}\widetilde{\psi} + r^{-1}(rV_b)'\mathrm{i}k\widetilde{\phi}, \tag{3.5a}$$

$$0 = \{(\delta^{-2}\partial_Y^2 - k^2) - \sigma - \mathrm{i}mr^{-1}V_b\}(\delta^{-2}\partial_Y^2 - k^2)\widetilde{\phi} - 2\mathrm{i}kr^{-1}V_b\widetilde{\psi}, \tag{3.5b}$$

from which we find the balance $m(V_b/r) \sim \delta^{-2}$ for non-axisymmetric disturbances. Because we already know that the instability appears near the inner wall, it is convenient to choose $\bar{r} = r_i$ and seek an asymptotic structure in a layer where $Y = \delta^{-1}(r - r_i) \sim O(1)$, where the layer thickness is $\delta = G^{-1/5}$ with $G = r_i^{-1}8A^2 \gg 1$, similar to the previous section. Substituting the scaled quantities $Q_0 = -V_b|_{r=r_i}/(2\delta A)$, $m_0 = 2Am\delta^3/r_i$, $\sigma_0 = \delta^2\sigma$, $k_0 = \delta k$ and the potential expansions $\widetilde{\phi} = \delta^{-1}\widetilde{\phi}_0 + \cdots$, $\widetilde{\psi} = 2A\widetilde{\psi}_0 + \cdots$ into (3.2), we get the leading-order equations

$$0 = \{(\partial_Y^2 - k_0^2) - \widetilde{\sigma}_0 + \mathrm{i}m_0(Q_0 - Y)\}\widetilde{\psi}_0 + \mathrm{i}k_0\widetilde{\phi}_0, \tag{3.6a}$$

$$0 = \{(\partial_Y^2 - k_0^2) - \widetilde{\sigma}_0 + \mathrm{i}m_0(Q_0 - Y)\}(\partial_Y^2 - k_0^2)\widetilde{\phi}_0 + \mathrm{i}k_0(Q_0 - Y)\widetilde{\psi}_0. \tag{3.6b}$$

Here it is important to notice that (3.6) does not explicitly depend on η, meaning that the solution of this canonical problem describes the rapidly counter-rotating asymptotic limit of the neutral curve for all η. This system is of course a natural generalisation of (2.9) and we can solve it numerically to seek neutral values $Q_0(m_0, k_0)$. The global minimum of $Q_0(m_0, k_0)$ is the critical value that gives the asymptotic prediction of the neutral curve. The computational result shown in figure 6(*a*) reveals that the minimum is at $(Q_0, k_0, m_0) = (3.85, 0.300, 0.315)$, as shown by the circle. The fact that the minimum is at $m_0 \neq 0$ explains why we observe spiral disturbances near the neutral curve in the counter-rotating case. Having determined the critical value, then by definition of the scaled parameters we have the leading-order asymptotic results

$$R_i = C_2|R_o|^{3/5}, \quad k = k_0 g^2 |R_o|^{2/5}, \quad m = \sqrt{2r_i}m_0 g|R_o|^{1/5}, \tag{3.7a–c}$$

https://doi.org/10.1017/jfm.2016.660 Published online by Cambridge University Press

where

$$g(\eta) = \left(\frac{8(1-\eta)}{\eta(1+\eta)^2} \right)^{1/10}, \quad C_2(\eta) = Q_0 g^3 \sqrt{\frac{r_i}{2}}, \tag{3.8a,b}$$

describe the non-trivial dependence of the asymptotic stability on η. Here we have used the fact that $|R_o| \gg |R_i|$ in the limit.

In figure 1 the asymptotic result is compared with the full Navier–Stokes result for $\eta = 5/7$. The asymptotic prediction given by (3.7), the red solid curve, is in excellent agreement with the rapid counter-rotation limit of the full neutral curve. For other values of the radius ratio, the convergence has been checked by comparing the full Navier–Stokes neutral value of $R_i|R_o|^{-3/5}$ at sufficiently large $-R_o$ with its asymptotic value C_2 in (3.8). We can see in figure 6(*b*) that the asymptotic result derived here predicts well the full computational result over a wide range of η, although the approximation gets slightly worse for small η because the optimum value of m is restricted to be an integer value in the full computation.

4. Conclusion and discussion

An asymptotic theory is developed for the neutral curve of Taylor–Couette flow. The analysis is mathematically consistent with the rapid-rotation limit of the Navier–Stokes equations, in contrast to previous works based on a fully empirical model approach (Esser & Grossmann 1996; Dutcher & Mullar 2007).

Our theory is first derived for the axisymmetric disturbances for the narrow-gap limit ($\eta \to 1$) and then extended to the general case. Here we briefly discuss the implications of the results in § 2 since, although the limiting equations (2.6) were derived and solved in, for example, Drazin & Reid (1981), the convergence of the wide-gap neutral curve to this limit has not been discussed. In order to observe the convergence, we found that the rescaled Reynolds numbers (2.7) must be used, as seen in figure 2. Here we further remark that the convergence can be observed even when the disturbances are non-axisymmetric. For the non-axisymmetric case, we must scale the azimuthal wavenumber m so that the azimuthal convective terms balance with the viscous terms, namely $Am/\bar{r} \sim O(\bar{r}^0) \sim O((1-\eta)^{-1})$. In the limit, the problem reduces to the Cartesian problem and the streamwise wavenumber $\alpha \equiv m/\bar{r}$ is $O(\bar{r}^{-1/2})$ since $A \sim O(\bar{r}^{1/2})$ from (2.3) and (2.7). This means that the streamwise scale is much longer than the gap, and thus the limiting equations are similar to the Görtler vortex equations derived by Hall (1983), i.e. the streamwise derivatives in the pressure and viscous terms are dropped from the Navier–Stokes equations for unit Reynolds number; these equations are also called boundary region equations, see Deguchi, Hall & Walton (2013), for example. When the neutral curve is close to the Rayleigh line, the narrow-gap limit becomes RPCF, and this is the special case where there is a degree of freedom in choosing the scaling of the Reynolds numbers because we do not need to balance the term proportional to G in (2.6). The freedom can be removed by further assuming that the Navier–Stokes equations are recovered in the limit, and this is in fact the case studied by Nagata (1986). This assumption requires $\alpha \sim O(\bar{r}^0)$, and thus $\overline{V}/\bar{r}$, R_i, R_o are $O(\bar{r}^0)$ quantities as well.

The high-Reynolds-number asymptotic analysis is performed assuming the size of A and B, which appear in the basic flow (2.3). From observation of the Rayleigh discriminant, it is obvious that a neutral asymptotic structure is possible when $|A|$ is small and $|B|$ is large, as long as $|AB|$ is $O(1)$. The smallness of $|A|$ means that

https://doi.org/10.1017/jfm.2016.660 Published online by Cambridge University Press

we are concerned with the neutral curve near the Rayleigh line, where the cylinders are corotating and the most unstable disturbance is known to take an axisymmetric form. In the asymptotic limit, we can compute the critical value of AB, which gives a viscous correction of the neutral curve from the Rayleigh line (3.3). Although the correction is asymptotically small, it is important, because our analysis showed that the neutral disturbance is fully viscous even when the cylinders rotate asymptotically fast.

For the counter-rotating case, the neutral curve can be described by the asymptotic problem obtained when $|A|$ is large and $|R_i/R_o|$ is small. The asymptotic problem for the counter-rotating case can be derived by considering the thin layer near the inner cylinder. It is only in that layer that the Rayleigh discriminant remains positive and thus the vortices are localised. This asymptotic vortex structure is quite different from that for the corotating limit, occupying the whole gap. Within the layer, asymptotic balance gives the non-trivial asymptotic behaviour $R_i \propto R_o^{3/5}$, $k \propto R_o^{2/5}$ and $m \propto R_o^{1/5}$. Further analysis gives an analytic expression for the neutral curve, with the coefficients fixed by the numerical computation of the canonical asymptotic problem, valid for all η, as shown in (3.6). The asymptotic result predicts that the most unstable mode is non-axisymmetric, consistent with the fact that spiral vortices are observed in the counter-rotating Taylor–Couette experiments.

The present linear results may also be important in building asymptotic theories for nonlinear vortices in Taylor–Couette flow, where the torque scaling is a matter of great concern for recent experiments. When the amplitude of the disturbance is $O(1)$ or less, a nonlinear theory can be found by a simple extension of the viscous linear theory here. For larger amplitudes, the viscous nonlinear asymptotic structure may break down to produce inviscid vortices at the asymptotic limit. It is noteworthy that, from the form of (2.2), such inviscid vortices naturally develop the zero-absolute vorticity states observed, for example, in Johnston, Halleen & Lezius (1972); see appendix A. In that inviscid case, the viscous layer must appear around the cell perimeter to satisfy the boundary conditions, as seen in the high-Reynolds-number direct numerical simulations (see Ostilla *et al.* 2013, for example). The three-dimensional extension of such a fully nonlinear theory is also of interest since it may describe the nonlinear structures that could even reach the Rayleigh stable region (Deguchi *et al.* 2014).

Appendix A. The emergence of zero-absolute vorticity states

Here we prove that inviscid Taylor vortices create so-called zero-absolute vorticity states, extending the standard argument of the Prandtl–Batchelor theorem; see Batchelor (1967) for example. Consider the axisymmetric Navier–Stokes equations (2.2) and define the modified steady streamfunction $\widehat{\varphi} \equiv r\varphi$, azimuthal velocity $\widehat{V} \equiv rV$ and azimuthal vorticity $\widehat{\omega} \equiv -r^{-1}\Delta\varphi$. We assume that the viscous terms in (2.2) are small and the contour of $\widehat{\varphi}$ is closed. Let us focus on the contour defined by fixing $\widehat{\varphi}$ as some constant. The key is the integration of (2.2*a*) over the area $\mathcal{A}$ enclosed by the contour. First, if we transform (r, z) to coordinates (n, s) that are normal and tangential to the contour, we see that $\widehat{V}$ is a function of n only; note that since the convective term dominates the inviscid flow, along the contour $0 \approx \widehat{\varphi}_n\widehat{V}_s - \widehat{\varphi}_s\widehat{V}_n = \widehat{\varphi}_n\widehat{V}_s$ and thus $\widehat{V}_s \approx 0$ to leading order. Then the integral of (2.2*a*) can be evaluated as

$$0 = \int_{\mathcal{A}} [(r^{-1}\widehat{V}_r)_r + r^{-1}\widehat{V}_{zz}]\,\mathrm{d}r\,\mathrm{d}z = \widehat{V}'(n) \oint_{\partial\mathcal{A}} r^{-1}\,\mathrm{d}s, \tag{A 1}$$

https://doi.org/10.1017/jfm.2016.660 Published online by Cambridge University Press

that is, $\widehat{V}'(n) = 0$ and we conclude that $\widehat{V}$ is a constant in the region where the assumptions hold. Similar arguments can be used for (2.2*b*) to prove that $\widehat{\omega}$ is constant there as well. The constancy of $\widehat{V}$ means that the axial absolute vorticity $r^{-1}(rV)_r$ is zero.

References

ANDERECK, C. D., LIU, S. S. & SWINNEY, H. L. 1986 Flow regimes in a circular Couette system with independently rotating cylinders. *J. Fluid Mech.* **164**, 155–183.

BATCHELOR, G. K. 1967 *An Introduction to Fluid Dynamics*. Cambridge University Press.

BOYD, J. P. 2001 *Chebyshev and Fourier Spectral Methods*. Dover.

DEGUCHI, K., HALL, P. & WALTON, A. G. 2013 The emergence of localized vortex–wave interaction states in plane Couette flow. *J. Fluid Mech.* **721**, 58–85.

DEGUCHI, K., MESEGUER, A. & MELLIBOVSKY, F. 2014 Subcritical equilibria in Taylor–Couette flow. *Phys. Rev. Lett.* **112**, 184502.

DEGUCHI, K. & NAGATA, M. 2011 Bifurcations and instabilities in sliding Couette flow. *J. Fluid Mech.* **678**, 156–178.

DRAZIN, P. G. & REID, W. H. 1981 *Hydrodynamic Stability*. Cambridge University Press.

DUTCHER, C. S. & MULLAR, S. J. 2007 Explicit analytic formulas for Newtonian Taylor–Couette primary instabilities. *Phys. Rev.* E **75**, 047301.

ESSER, A. & GROSSMANN, S. 1996 Analytic expression for Taylor–Couette stability boundary. *Phys. Fluids* **8**, 1814–1819.

GROSSMANN, S., LOHSE, D. & SUN, C. 2016 High-Reynolds number Taylor–Couette turbulence. *Annu. Rev. Fluid Mech.* **48**, 53–80.

HALL, P. 1982 Taylor–Görtler vortices in fully developed or boundary layer flows: linear theory. *J. Fluid Mech.* **124**, 475–494.

HALL, P. 1983 The linear development of Görtler vortices in growing boundary layers. *J. Fluid Mech.* **130**, 41–58.

JOHNSTON, J. P., HALLEEN, M. & LEZIUS, D. K. 1972 Effects of spanwise rotation on the structure of two-dimensional fully developed turbulent channel flow. *J. Fluid Mech.* **56**, 533–557.

LANGFORD, W. F., TAGG, R., KOESTLICH, E. J., SWINNEY, H. L. & GOLUBITSKY, M. 1988 Primary instabilities and bicriticality in flow between counter-rotating cylinders. *Phys. Fluids* **31**, 776–785.

NAGATA, M. 1986 Bifurcations in Couette flow between almost corotating cylinders. *J. Fluid Mech.* **169**, 229–250.

OSTILLA, R., STEVENS, R. J. A. M., GROSSMANN, S., VERZICCO, R. & LOHSE, D. 2013 Optimal Taylor–Couette flow: direct numerical simulations. *J. Fluid Mech.* **719**, 14–46.

RAYLEIGH, LORD 1917 On the dynamics of revolving fluids. *Proc. R. Soc. Lond.* A **93**, 148–154.

TAYLOR, G. I. 1923 Stability of a viscous liquid contained between two rotating cylinders. *Phil. Trans. R. Soc. Lond.* A **223**, 289–343.

VERONIS, G. 1970 The analogy between rotating and stratified fluids. *Annu. Rev. Fluid Mech.* **2**, 37–66.

https://doi.org/10.1017/jfm.2016.660 Published online by Cambridge University Press